Thermochronology and U–Pb dating of detrital zircons from the Demerara Plateau (French Guiana-Suriname): Implications for the provenance of the Early Cretaceous syn-rift sedimentation

Igor Girault, Christophe Basile, Matthias Bernet, Jean-Louis Paquette, Arnauld Heuret, Lies Loncke, Ewald Poetisi, Mélanie Balvay

Received: 20 February 2022 | Revised: 15 January 2023 | Accepted: 31 January 2023

DOI: 10.1111/bre.12758

Basin Research | IAS EAGE | WILEY

RESEARCH ARTICLE

Thermochronology and U–Pb dating of detrital zircons from the Demerara Plateau (French Guiana-Suriname): Implications for the provenance of the Early Cretaceous syn-rift sedimentation

Igor Girault[1] | **Christophe Basile**[1] | **Matthias Bernet**[1] | **Jean-Louis Paquette**[2] | **Arnauld Heuret**[3] | **Lies Loncke**[4] | **Ewald Poetisi**[5] | **Mélanie Balvay**[1]

[1]Université Grenoble Alpes, Université Savoie Mont Blanc, CNRS, IRD, IFSTTAR, ISTerre, Grenoble, France

[2]Université de Clermont Auvergne, CNRS, IRD, OPGC, Laboratoire Magmas et Volcans, Clermont-Ferrand, France

[3]Université de Guyane, Géosciences Montpellier, Cayenne, France

[4]Université de Perpignan, CEFREM (UMR 5110), Perpignan, France

[5]Anton de Kom University of Suriname, Paramaribo, Suriname

Correspondence
Igor Girault, Université Grenoble Alpes, Université Savoie Mont Blanc, CNRS, IRD, IFSTTAR, ISTerre, Grenoble, France.
Email: igor.girault@neuf.fr

Present address
Igor Girault, IDEES (UMR 6266), Université de Rouen, Rouen, France

Abstract

The provenance of Early Cretaceous sandstones dredged on the northern margin of the Demerara Plateau, offshore French Guiana and Suriname, reveals the sediment routing system that prevailed through the Equatorial Atlantic rifting. Fission-track analysis and U–Pb dating of 310 and 111 detrital zircons, respectively, have been performed. Microfacies analysis and inherited cooling ages suggest that the sandstones were deposited in shallow marine environments during the Early Cretaceous, before the Late Albian drowning of the marginal plateau. Most of the U–Pb zircon crystallisation ages are comprised of between 700 and 600 Ma and are attributed to the Pan-African-Brasiliano orogeny. Statistical and chronological evidence suggest that the zircon fission-track cooling ages were inherited from source materials. Triassic peak ages (>50% of the population) are attributed to the early phase of Central Atlantic rifting. One sample records a cooling phase at ca. 170 Ma, presumably following volcanic hotspot activity and the opening of the Central Atlantic Ocean. Two other samples record the rapid exhumation of the French Guiana transform margin during the Equatorial Atlantic rifting (127 ± 11 and 106 ± 8 Ma). We propose a source-to-sink model in which the Pan-African-Brasiliano basement of the margin was eroded as a result of flexural uplift along the French Guiana margin, and the detrital material funnelled in the Cacipore graben sustained the Early Cretaceous syn-rift sedimentation on the marginal plateau.

KEYWORDS

Demerara Plateau, provenance analysis, source-to-sink, thermochronology, transform margin

1 | INTRODUCTION

The opening of the Atlantic Ocean resulted from the diachronous break-up of the supercontinent Pangea. The first phase of rifting occurred between North America and Gondwana during the Early Jurassic, leading to the opening of the Central Atlantic Ocean (Sahabi et al., 2004; Labails et al., 2010). The South and Equatorial Atlantic Oceans later opened during the Early Cretaceous, following a second phase of rifting between South America and Africa (Basile et al., 1998; Basile et al., 2005; Moulin et al., 2010).

The Demerara Plateau is a marginal plateau extending up to 400 km offshore French Guiana and Suriname, at the former triple junction between North America, South America and Africa (Figure 1a,b). Along with its African conjugate margin, the Guinea Plateau, it therefore represents a key area in the understanding of the opening of the Equatorial Atlantic Ocean (Basile et al., 2005; Basile et al., 2022; Benkhelil et al., 1995; Gouyet, 1988; Graindorge et al., 2022; Loncke et al., 2022; Loparev et al., 2021; Olyphant et al., 2017).

The structure of the Demerara Plateau is well documented by multiple sets of seismic data (Basile et al., 2013; Casson et al., 2021; Gouyet, 1988; Graindorge et al., 2022; Greenroyd et al., 2008; Loncke et al., 2016; Loncke et al., 2022; Loparev et al., 2021; Mercier de Lépinay, 2016; Museur et al., 2021; Reuber et al., 2016). By contrast, the petrological data reported in the academic literature are rather scarce. Previous authors have described several sedimentary cores as well as industrial wells penetrating the Early Cretaceous syn-rift sequence (Casson et al., 2021; Erbacher et al., 2004; Gouyet, 1988; Hayes et al., 1972; Loncke et al., 2022; Mercier de Lépinay, 2016). Among them, only one industrial well has reached the pre-rift deposits (Casson et al., 2021; Gouyet, 1988; Loncke et al., 2022; Mercier de Lépinay, 2016). In addition, a single dredge previously yielded Late Jurassic to Early Cretaceous deposits (Fox et al., 1970).

Provenance analysis aims at locating the source areas of detrital sediments based on a wide range of petrological evidence (Boggs Jr, 2009). Over the past decade, provenance analysis of heavy minerals has emerged as a powerful tool for reconstructing the tectono-sedimentary evolution of rift basins (Baesso et al., 2021; Hart et al., 2016; Olierook et al., 2019; Wang et al., 2021). So far, the scarcity of coarse detrital material precluded a provenance analysis of pre-break-up deposits of the Demerara Plateau. The oceanographic research campaign DRADEM (Basile et al., 2016) was carried out in 2016 in order to sample pre-break-up material by dredging along the Equatorial Atlantic margin of the plateau. Among the eight successful dredges, several yielded coarse detrital rocks. This study aims to characterising the depositional environments and provenance of the deposits.

Highlights

- Sandstones were dredged on the Equatorial Atlantic transform margin of the Demerara Plateau.
- Depositional environments and zircon fission-track cooling ages bracket the depositional ages.
- Detrital zircon fission-track cooling ages recorded syn-transform margin exhumation.
- Provenance analysis suggests a 650 Ma old Pan-African orogen as basement of the Equatorial Atlantic margin.

2 | GEOLOGICAL SETTING

2.1 | Plate kinematics

The Demerara Plateau is bordered to the west by the Guyana basin, part of the Central Atlantic Ocean, and to the east by the Equatorial Atlantic Ocean. The plateau is delimited to the east and west by two divergent margins, and to the north by a steeper, transform margin (Figure 1b). The segmentation of the plateau results from the superimposition of successive phases of rifting (Gouyet, 1988; Graindorge et al., 2022; Loncke et al., 2022; Loparev et al., 2021; Mercier de Lépinay, 2016; Museur et al., 2021; Reuber et al., 2016).

The western divergent margin of the Demerara Plateau formed during the Central Atlantic rifting, as a result of NW-SE divergence between North America and Gondwana (Figure 1c). Interpretation of ocean floor magnetic anomalies suggests that oceanic accretion started in the Central Atlantic during the Late Sinemurian, ca. 190 Ma (Labails et al., 2010; Sahabi et al., 2004). However, the onset of oceanic accretion is not well constrained in the Guyana basin and could have occurred later. Nemčok et al. (2015) proposed a Late Jurassic age as an upper bound based on the correlation of seismic data with stratigraphic evidence from the industrial well.

During the Early Cretaceous, the Equatorial Atlantic rift opened with an ESE-WNW divergence, forming the eastern divergent margin of the plateau. The Central Atlantic margin was sheared between the Demerara Plateau and the Guinea Plateau, forming two dextral, conjugate transform margins (Basile et al., 2022; Basile et al., 2013; Figure 1d). Dating of deposits from the Benue basin and the Ivory-Coast-Ghana Plateau indicate that the Equatorial Atlantic rifting started during the Early Barremian, ca. 129 Ma (Basile et al., 2005; Brunet et al., 1988) and the onset of oceanic accretion occurred during the Late Aptian, ca. 114 Ma (Basile et al., 1998; Basile et al., 2005; Moulin et al., 2010).

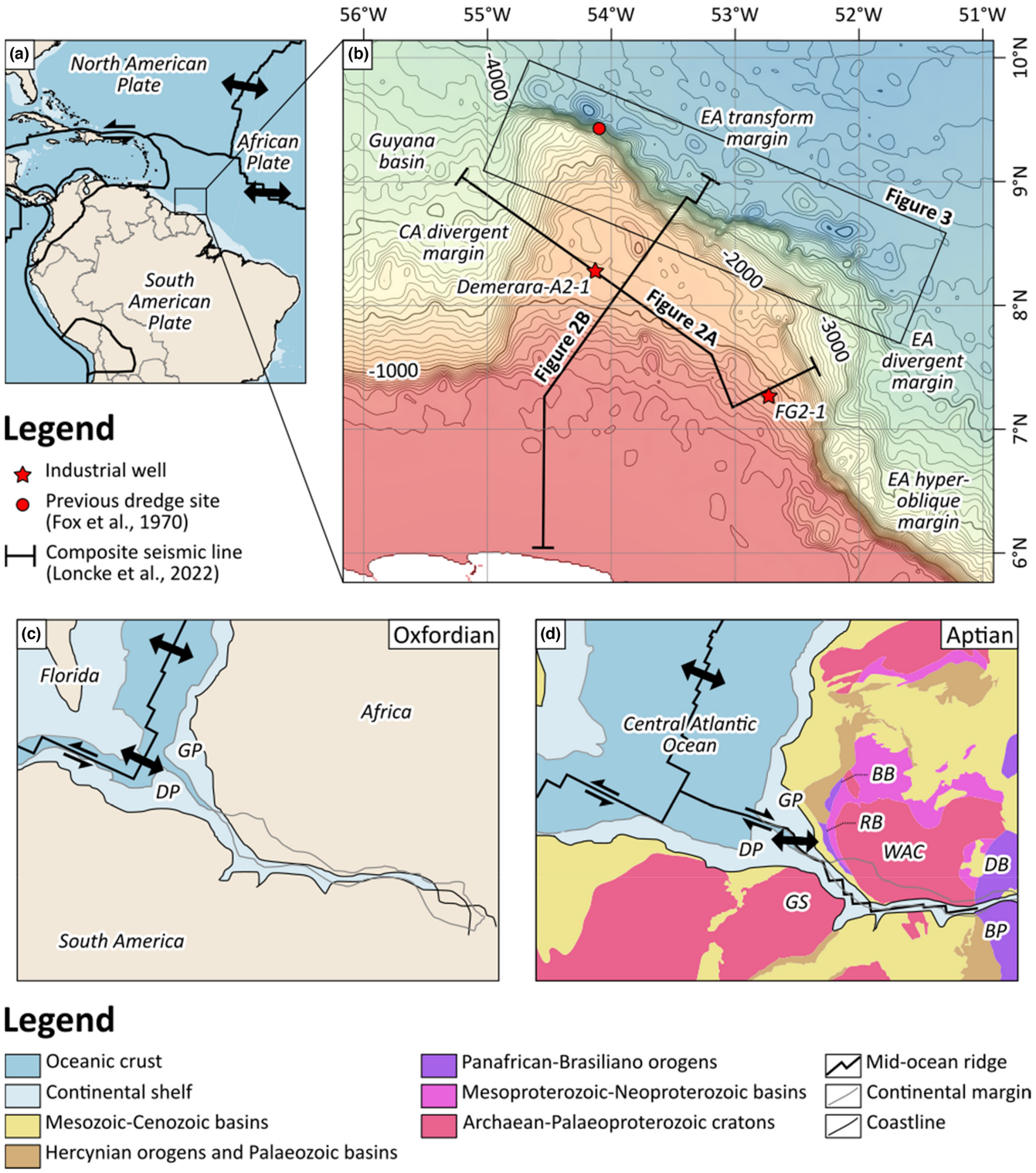

FIGURE 1 Geological setting of the Demerara Plateau. (a) Present-day setting. (b) Bathymetric map of the Demerara Plateau and location of seismic lines, Demerara-A2-1 and FG2-1 wells. CA: Central Atlantic; EA: Equatorial Atlantic. Bathymetric data from Amante & Eakins, 2009. (c) Palaeogeographical reconstruction of the southern Central Atlantic Ocean during the Oxfordian, ca. 40 Myr after the onset of oceanic accretion. Modified from Reuber et al., 2016. (d) Palaeogeographical reconstruction of the southern Central Atlantic Ocean during the Aptian, at the onset of Equatorial Atlantic rifting. DP: Demerara Plateau; GP: Guinea Plateau; GS: Guiana shield; WAC: West African craton; BP: Borborema Province; BB: Bassaride belt; DB: Dahomeyide belt; RB: Rockelide belt. Modified from Reuber et al. (2016). Geological data from Thiéblemont et al. (2016) for Africa and Gómez et al. (2019) for South America.

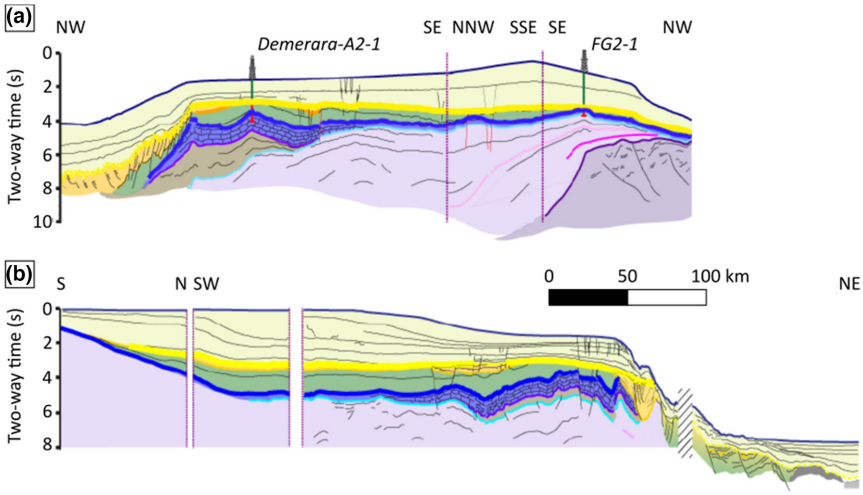

Legend

	Lithology	Main unconformities	Age
	Clay and chalk (pelagic deposits)	Uc8 (Late Albian unconformity)	Since the Late Albian
Unit F		Uc7	Albian
Unit E	Sandstone (deltaic deposits)	Uc6	Aptian
Unit D	Limestone (carbonate platform)		Pre-Tithonian-Barremian
Unit C			
Unit B	Volcanic rocks (Seaward Dipping Reflectors)		Early Jurassic?
Unit A	Plutonic and metamorphic rocks		Precambrian?

FIGURE 2 Structure of the Demerara Plateau. (a) SW–NE seismic line interpretation. (b) NW-SE seismic line interpretation. Modified from Loncke et al. (2022).

2.2 | Stratigraphic record

2.2.1 | Previous works

Mercier de Lépinay (2016) and Loncke et al. (2022) defined seven geological units in the Demerara Plateau (Figure 2), based on an extensive compilation of seismic data. The age and lithology of these units are constrained by four sedimentary cores (Erbacher et al., 2004; Hayes et al., 1972), as well as four industrial wells (Gouyet, 1988; Loncke et al., 2022; Mercier de Lépinay, 2016) recently re-evaluated by Casson et al. (2021).

2.2.2 | Basement

Units A and B represent the basement of the Demerara Plateau, defined as the units predating the Central Atlantic break-up (Casson et al., 2021; Loncke et al., 2022). Unit A has been penetrated by the Sinnamary-1 well, which yielded cuttings attributed to the Guyana Shield (Loncke et al., 2022; Mercier de Lépinay, 2016). This unit is laterally overlapped by a 21-km-thick unit referred to as Unit B by Mercier de Lépinay (2016) and Loncke et al. (2022). Recent works (Graindorge et al., 2022; Loncke et al., 2022; Loparev et al., 2021; Mercier de Lépinay, 2016; Museur et al., 2021; Reuber et al., 2016) have shown that Unit B is characterised by Seaward Dipping Reflectors (SDR; Figure 2a), a distinctive feature of volcanic passive margins (Geoffroy, 2005; Roberts et al., 1984). It is therefore interpreted as composed of Jurassic syn-rift volcanic material. Whether this material erupted in synchronicity with the Central Atlantic Magmatic Province ca. 201 Ma (Marzoli et al., 1999; Marzoli et al., 2018) or later is debated (Reuber et al., 2016). In support of the latter hypothesis, rhyolite samples dredged on the Demerara Plateau recently yielded a U–Pb age of 173 ± 2 Ma (Basile et al., 2022).

2.2.3 | Pre-Cretaceous-rifting deposits

Unit B is overlain by a sedimentary unit (Unit C) restricted to the western part of the plateau (Figure 2a). The lithology remains uncertain in the absence of sampling reported in the academic literature (Loncke et al., 2022). Unit C is overlapped by a carbonate platform (Unit D), partially penetrated by the Demerara-A2-1 well (Gouyet, 1988; Figure 2a). Limestones at the base of the well were dated as Tithonian based on nannofossil and calpionellid assemblages (Casson et al., 2021).

2.2.4 | Syn-Cretaceous-rifting deposits

Unit D is truncated by an erosional unconformity (Uc6; Loncke et al., 2022). In the FG2-1 well, Uc6 truncates ferruginous sandstones overlaying Barremian basalts, which suggests subaerial erosion (Casson et al., 2021; Gouyet, 1988). Uc6 is overlain by interbedded deltaic sandstones (the Stabroek Formation; Casson et al., 2021) and mudstones, referred to as Unit E. This unit is characterised by fan-shaped reflectors indicating syn-rift sedimentation (Loncke et al., 2022). Unit E is truncated by several unconformities. The lowest of them (Uc7) is overlain by Unit F. This unit is not preserved in most of the plateau and has not been penetrated by the industrial wells reported in the academic literature (Loncke et al., 2022).

2.2.5 | Post-Cretaceous-rifting deposits

The pre-rift and syn-rift units are deformed by syn-rift normal faults and syn-transform folds (Basile et al., 2013; Loncke et al., 2022; Mercier de Lépinay, 2016; Sapin et al., 2016; Figure 2b). These deformations are sealed by a Late Albian erosional unconformity (Uc8), truncating the older units down to the Precambrian basement in the eastern part of the plateau (Loncke et al., 2022; Mercier de Lépinay, 2016). The associated uplift is evaluated to ca. 1 km (Casson et al., 2021). Uc8 has been initially interpreted as a post-transform unconformity (Basile et al., 2013; Gouyet, 1988). Alternately, Basile et al. (2022) suggested that the uplift was caused by an Early Cretaceous hotspot swell. In support of this hypothesis, several industrial wells document volcanic activity during the Barremian, on the Demerara Plateau (Gouyet, 1988) and during the Aptian-Albian, on the Guinea Plateau (Olyphant et al., 2017).

Uc8 marks the last episode of denudation on the Demerara Plateau. It is overlain by pelagic deposits (Unit G), attesting to the thermal subsidence of the margin and subsequent drowning of the plateau (Erbacher et al., 2004; Fanget et al., 2020).

3 | MATERIALS

3.1 | Sampling strategy

According to seismic data, pre-break-up units outcrop along the transform margin of the plateau. The aim of the DRADEM cruise was to sample the outcropping material by dredging the sea floor. The cruise was carried out on board the French oceanographic vessel *Pourquoi pas*? in July 2016 (Figure 3a). Six dredge sites were successful. Three of them yielded coarse detrital sediments: sites A, B and F. In addition, other dredge sites yielded Middle Jurassic magmatic rocks (Basile et al., 2020), pre-Late Albian calcareous breccia and Rupelian chalk (Girault, 2017).

3.2 | Site A: Come Back Canyon

Site A is located at the western extremity of the northern slope of the Demerara Plateau, 20 km west of the site previously dredged by Fox et al. (1970). The dredge DRA-A1 was carried out at 4200–4400 m depth in a canyon named 'Come Back Canyon' (Figure 3b). Close to the starting point, the dredge got stuck, forcing the vessel to come back above the dredge to release it from the sea floor. This position (at ca. 4350 m depth) is interpreted as the sampling location of in situ bedrock.

The dredge collected 40 rock fragments with a mass ranging from 80 g to 30.8 kg. Several fragments present surfaces covered by a millimetre-thin crust of iron and manganese oxides, hence interpreted as formerly outcropping on the sea floor. In contrast, the other surfaces are not weathered and are interpreted as fractures caused by dredging. Correlation with seismic line located 7 km to the west suggests that the samples were collected below the Late Albian unconformity (Uc8; Figure 3c).

3.3 | Site B: Waste canyon

Site B is located on the northern slope of the plateau, 24 km east of the site dredged by Fox et al. (1970). Dredging took place at 4000–4600 m depth, in a canyon named 'Waste Canyon' (Figure 3b). The dredge DRA-B1 yielded 37 fragments of sandstone with a mass of 20 g–6.6 kg. The fragments do not present fresh fractures, and the edges are slightly blunt. One sample was colonised by a living sea anemone, indicating that it was not buried. Hence, we interpret the rock fragments dredged in the Waste Canyon as submarine screes. Correlation with a seismic line located 6 km to the east suggests that the samples were collected below the Late Albian unconformity (Uc8; Figure 3c).

3.4 | Site F: Goleador Hill

Site F is located at the intersection of the northern and eastern margins of the plateau, on an NNW–SSE ridge culminating at ca. 3800 m deep and named 'Goleador Hill'. Dredge DRA-F1 was carried out at 4200–4000 m depth on the eastern side of the ridge (Figure 3b). Nine fragments of sandstone with a mass of 90 g–53.1 kg were collected. No significant rise in the cable tension occurred during dredging, which indicates that the samples showed no

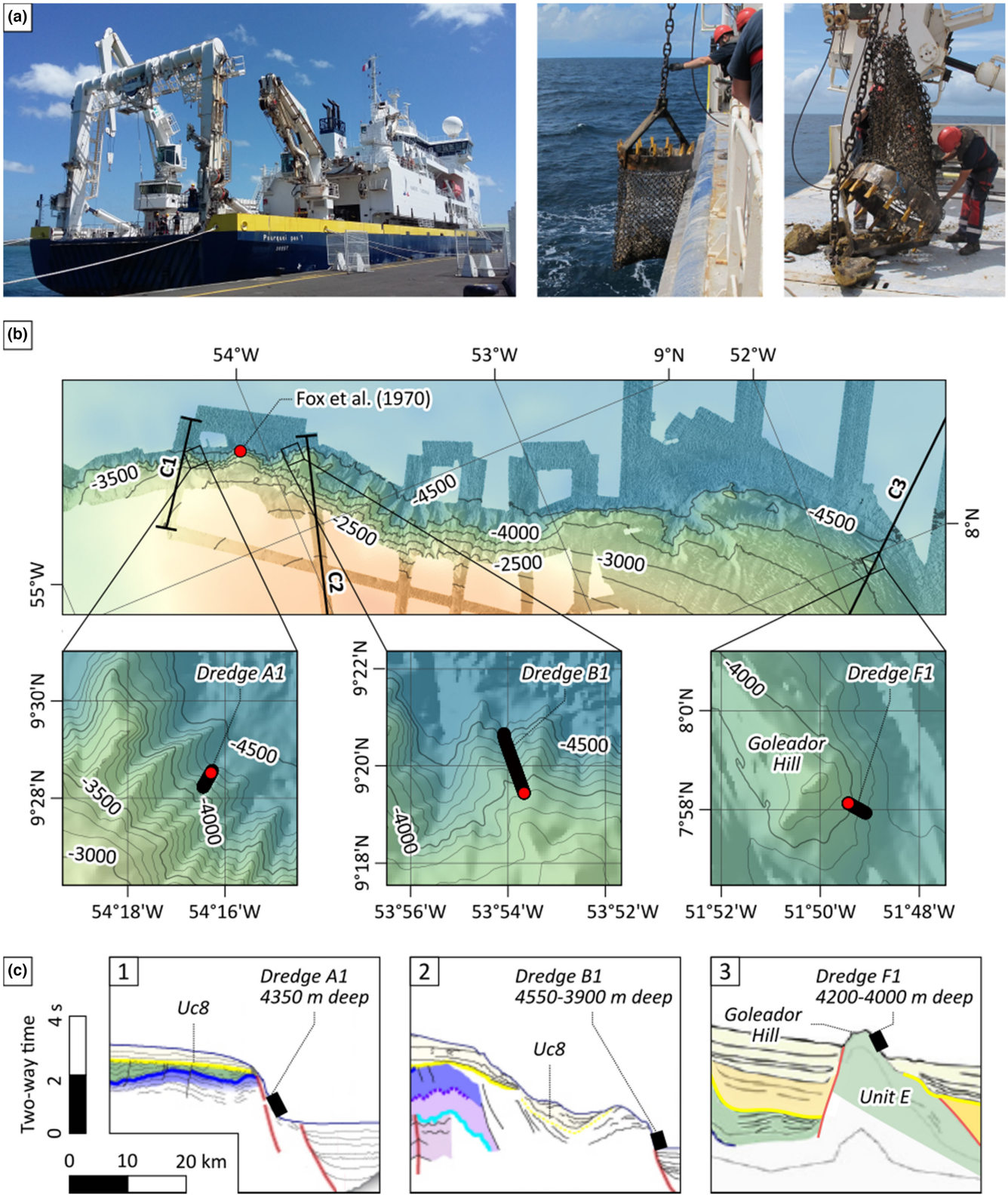

FIGURE 3 Sampling sites. (a) French oceanographic research vessel Pourquoi pas? and dredging operation (DRA-A1) during the DRADEM cruise, July 2016. (b) Bathymetric map of the northern slope of the Demerara Plateau and location of the DRA-A1, B1 and F1 dredges. Bathymetric data: GUYAPLAC, IGUANES and DRADEM cruises. (c) Projection of the dredges on close seismic lines. C1-2: modified from Loncke et al. (2022); C3: modified from Museur et al. (2021).

resistance to the dredge. After the break-up with a hammer, the section of the largest fragment (DRA-F1-1) presents a concentric alteration front formed by oxide precipitation and sea floor mica alteration to smectite (Girault, 2017). The fragments are therefore interpreted as submarine screes. Correlation with a seismic line located 1 km to the west suggests that the material is derived from unit E (Figure 3c).

4 | METHODS

4.1 | Microfacies analysis

Twelve sedimentary samples representative of the macroscopic facies and weathering stage diversity (Girault, 2017) were selected to realise 13 uncovered thin sections with a thickness of 30 µm. We used two samples from site A (two sections obtained from DRA-A1-4, and one from DRA-A1-17), seven from site B (DRA-B1-1, 2, 3, 4, 7, 25 and 27) and three from site F (DRA-F1-1, 7, and 8). The thin sections were made in the workshop of Lithologie Bourgogne, Saint-Apollinaire, France and systematically analysed with a polarised light microscope. Five microfacies were defined based on lithology, grain components, matrix, cement, depositional and deformation structures in order to reconstruct the depositional environments and diagenetic processes (Table 1). Complementary analyses were done with the Hitachi-S2500 Scanning Electron Microscope (SEM) and an Energy-Dispersive X-ray Spectroscopy (EDS) probe at the Institut des Sciences de la Terre (ISTerre), Université Grenoble Alpes, France. In addition, the mineralogical composition was assessed from X-Ray diffraction (XRD) analysis of the bulk sample powders with a Brucker D5000 X-Ray diffractometer at ISTerre. Mineral phases were identified and quantified using the DIDFFRAC.EVA software.

4.2 | Apatite and zircon fission-track analysis

4.2.1 | Rationale

Spontaneous fission of ^{238}U in minerals produces latent fission tracks, observable under an optical microscope after etching. Fission tracks accumulate in apatite and zircon crystals over time as long as the crystals remain below the effective closure temperature. The effective closure temperature depends primarily on the cooling rate. In the case of rapid, monotonic cooling (>15°C/Myr), the effective closure temperature is comprised in a range of 120 ± 20°C for apatite and 240 ± 20°C for zircon (Bernet et al., 2009; Brandon et al., 1998; Dodson, 1973; Reiners & Brandon, 2006). In the case of slow cooling (<2°C/Myr) or reheating of the rock due to burial or magmatic intrusion, partial annealing of the fission tracks occurs at temperatures below the effective closure temperature. The partial annealing zone (PAZ) temperature ranges from 60 to 114°C for a 10 Myr hold time in apatite and 180–240°C for a 10 Myr hold time in zircon (Reiners & Brandon, 2006). A population of 100 grains is necessary to approximate the representative cooling age spectrum of a detrital rock sample (Vermeesch, 2004).

4.2.2 | Sample preparation and cooling age calculation

The largest sedimentary samples of each dredge site (DRA-A1-6, DRA-B1-3 and DRA-F1-1) were selected for further preparation, in addition to magmatic samples from other dredges (DRA-C2-1 and a mixture of DRA-E1-2, 3, 4 and 8; Basile et al., 2020). The samples were processed in order to separate apatite and zircon grains at the Geo-Thermochronology laboratory of the Institute of Earth Sciences (ISTerre), Université Grenoble Alpes, France. The samples were crushed and sieved to the 80–200 µm fraction. Heavy minerals were concentrated using a Gemini separation table, and standard magnetic and heavy liquid separation techniques (Kohn et al., 2019). Magmatic samples appeared to be devoid of any apatite or zircon grain coarse enough for further analysis. In contrast, the sedimentary samples yielded 11 apatite grains (3 from DRA-B1-3 and 8 from DRA-A1-6) and 310 zircon grains (96 from DRA-A1-6, 94 from DRA-B1-3 and 120 from DRA-F1-1; Table 2; Table S1).

Apatite grains were mounted on epoxy resin and subsequently polished to expose internal grain surfaces. The surfaces were etched at 21°C for 20 s in a 5.5 mol HNO_3 solution. Zircon grains were mounted in Teflon® sheets. The grain mounts were polished and etched for 16–20 hours in a NaOH-KOH solution at 228°C, in order to reveal spontaneous fission tracks. We attached a low-U muscovite mica detector to each grain mount, following the external detector method for fission-track analysis. The samples were irradiated at the FRM II reactor of the Technische Universität München, in Garching, Germany, along with IRMM540R dosimeter glasses and Durango and Fish Canyon Tuff ages standards for apatite, and IRMM541 dosimeter glasses and Fish Canyon Tuff age standards for zircons. After irradiation, the mica detectors were attached for 18 minutes at 20°C in a 48% HF solution to reveal induced fission tracks. Both spontaneous and induced fission tracks were counted optically at a magnification of 1250 using an Olympus BH2 microscope and the FT-Stage 4.04 system. Cooling ages were calculated using the RadialPlotter Version 9.5 software (Galbraith & Green, 1990; Vermeesch, 2009).

TABLE 1 Microfacies of the pre-Late Albian detrital sedimentary rocks of the Demerara Plateau.

Code	Lithology	Grain components	Matrix	Cement	Depositional structures and bioturbation	Deformation structures	Depositional environment	Thin sections
Facies 1	Quartzarenite	Ooids with a core composed of sharp-edged angular quartz grains (100–200 μm) Mud clasts Bivalves Brachiopods Echinoderms Bryozoans	Micrite (restricted to the concave faces of bivalve shells)	Calcite isopachous cement Sparite	Cross bedding overlaying erosional surfaces	Pressure solution	Upper shoreface	DRA-A1-4a DRA-A1-4b DRA-A1-17
Facies 2	Quartzarenite	Sharp-edged angular to rounded quartz grains (50–200 μm) Bivalves Echinoderms Feldspath grains Plant debris	Micrite	Sparite Rhomboedric ankerite crystals	Plane bedding Burrows	—	Lower shoreface	DRA-B1-2 DRA-B1-3, DRA-B1-4 DRA-B1-7 DRA-B1-27
Facies 3	Quartzarenite	Rounded quartz grains (200–1000 μm)	—	Pore-filling quartz overgrowths Smectite	—	Pressure solution (microstylolites)	High-energy, marine to fluvial environment	DRA-F1-1 DRA-F1-7 DRA-F1-8
Facies 4	Quartzarenite	Corroded quartz grains (200 μm)	—	Goethite Quartz overgrowths	—	Micro-fractures	High-energy, marine to fluvial environment	DRA-B1-1
Facies 5	Shale	Quartz grains (<50 μm) Iron oxide framboids	Silt and clay	—	Laminae	—	Offshore	DRA-B1-25

Note: Terminology from Boggs Jr (2009) and Flügel (2009).

TABLE 2 Results of apatite and zircon fission-track analysis.

Mineral	Sample	Number of grains	ρ_s (105 cm-2)	n_s	ρ_i (105 cm-2)	n_i	ρ_d (105 cm-2)	Nd	P (ρ^2)	Dispersion (%)	Central age (Ma)	±2σ (Ma)	U (ppm)	±2σ (ppm)
Apatite	DRA-A1-6	8	3.6	119	5.65	188	10.3	4269	5.9	30.4	86	29	8	1
Apatite	DRA-B1-3	3	4.2	81	6.78	130	10.3	4277	14.7	0.7	86	24	10	2
Zircon	DRA-A1-6	96	101.0	13,942	9.22	1276	3.82	4009	0.0	43	244	34	121	8
Zircon	DRA-B1-3	94	96.0	14,659	10.20	1556	3.81	4008	0.0	44	215	30	134	8
Zircon	DRA-F1-1	120	76.7	17,454	9.39	2137	3.79	4008	0.0	44	176	22	124	7

Note: Fission tracks were counted dry at 1250× magnification using an Olympus BX51 microscope for apatite, an Olympus BH2 microscope for zircons and the FT-Stage 4.04 system. Apatite cooling ages were calculated using a zeta value of 268.76 ± 6.01 (M. Bernet) and the IRMM540R uranium glass standard (15 ppm U). Zircon cooling ages were calculated using a zeta value of 123.4 ± 4.82 (I. Girault) and the IRMM541 uranium glass standard (50 ppm U).

4.3 | Zircon U–Pb dating

Among the 310 zircon grains selected for fission-track analysis, 111 were selected for U–Pb dating: 23 from DRA-A1-6, 33 from DRA-B1-3 and 55 from DRA-F1-1. The grain sections were systematically observed under cathodoluminescence in order to locate variations of the chemical composition resulting from discontinuous crystallisation phases. We measured the $^{206}Pb/^{238}U$ and $^{207}Pb/^{235}U$ isotope ratios on the outermost growth ring of each zircon grain in order to date the last phase of crystallisation of the grain (Figure 4).

U–Pb isotope ratios were measured by in situ laser ablation inductively coupled plasma spectrometry (LA-ICP-MS) at the Laboratoire Magmas & Volcans in Clermont-Ferrand, France. We used a Resonetics Resolution M-50 Excimer laser system operating at a wavelength of 193 nm with a repetition rate of 3 Hz and a laser fluencce of 2.5 J.cm^{-2} for mineral ablation. The laser spot diameter was set at 20–27 µm. The ablated material was carried by helium and mixed with nitrogen and argon before injection into the plasma source of a Thermo Element XR sector-field HR-ICP-MS (Hurai et al., 2010; Mullen et al., 2018; Paquette et al., 2014). Measured U–Pb isotope ratios were corrected by standard bracketing with repeated measurements of GJ-1 zircon (Jackson et al., 2004) in order to avoid biases caused by U–Pb fractionation during laser sampling and instrumental mass discrimination. The 91,500 zircon reference material (Wiedenbeck et al., 1995) was repeatedly analysed in order to independently monitor the reproducibility and accuracy of the corrections.

Data reduction was carried out with the GLITTER software from Macquarie Research Ltd (van Achterbergh et al., 2001). Data were not corrected for common Pb. Concordia ages and diagrams were generated using the Isoplot/Ex v. 2.49 software (Ludwig, 2001).

5 | RESULTS

5.1 | Microfacies

5.1.1 | Facies 1: Calcareous sandstone

The samples collected by the DRA-A1 dredge consist of sandstone fragments with cross beddings (Figure 5a) overlaying erosional surfaces with truncated particles (Figure 5b). Grains are composed of ooids (90%) and bioclasts (10%). Ooids present a core composed of sharp-edged angular, well-sorted (100–200 µm) quartz grains covered by a 10–20 µm thin cortex. Bioclasts include bivalves (Figure 5c), brachiopods and rounded fragments

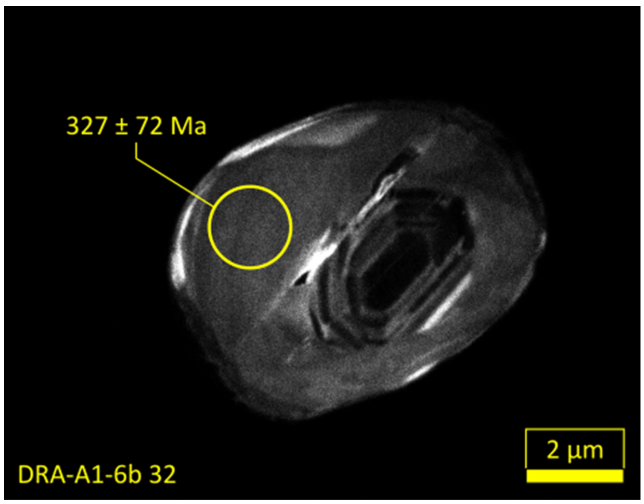

FIGURE 4 Example of the photograph of a detrital zircon grain under cathodoluminescence, highlighting successive crystallisation phases and location of the laser-ablated zone for dating.

of echinid radioles (Figure 5d) and bryozoan. Other elements include mudclasts (Figure 5e). Micritic matrix is rare and restricted to concave faces of bivalve shells (Figure 5c). The grains are covered by an isopachous calcite cement. Bivalves and ooids underwent pressure solution as they were punched by quartz grains under compaction (Figure 5f,g). Sparite eventually filled the intergranular porosity. These characteristics indicate that the sediment was deposited in a high-energy, shallow marine environment with strong detrital input, such as the upper shoreface zone of an epicontinental sea.

5.1.2 | Facies 2: Calcareous sandstone

Most samples recovered in dredge DRA-B1 (thin sections DRA-B1-2, 3, 4, 7 and 27) consist of sandstone fragments with planar beddings and millimetre-thin micritic interbeds. This sandstone is composed of well-sorted (50–200 µm), sharp-edged angular to rounded quartz grains (90%), in addition to feldspar, bioclasts including bivalves, echinoderms (Figure 5h) and plant fragments. Two samples (DRA-B1-14 and DRA-B1-27) present millimetre-thin layers composed of micrite. Intergranular porosity is filled mostly by micrite, alternatively with sparite and ankerite rhomboidal crystals. One sample (DRA-B1-2) is strongly bioturbated, presenting burrows up to 2 cm wide, filled by micrite (Figure 5i). These characteristics suggest that the sediment was deposited in a high-energy marine environment, yet with phases of micrite sedimentation, and strong detrital input, such as the lower shoreface zone of an epicontinental sea. One sample (DRA-B1-5) yielded the pollen genus *Afropollis* (Dall'Asta, personal communication). This genus is known on the Equatorial Atlantic African margin from the Late Barremian to the Middle Cenomanian (Moullade et al., 1998). This age is consistent with the seismic data indicating a pre-Late Albian age.

5.1.3 | Facies 3: Quartz-cemented sandstone

The samples collected by the DRA-F1 dredge consist of fragments of massive sandstone composed of coarse, well-sorted (200–1000 µm), subangular to rounded quartz grains (99%), in addition to muscovite. The intergranular porosity is totally filled by quartz outgrowths and smectite cement. Microstylolite contact between quartz grains indicates the rock underwent significant compaction and pressure solution (Figure 5j). In the absence of microfossil content, the depositional environment remains speculative, although compatible with a shallow marine as well as a deltaic environment.

5.1.4 | Facies 4: Ferruginous sandstone

This facies occurs in one sample from the DRA-B1 dredge (DRA-B1-1). This sample consists of a sandstone fragment made up of well-sorted (200 µm) quartz grains. The intergranular porosity is totally filled by goethite cement. Quartz grains present residual overgrowths mostly corroded and replaced by goethite cement. Quartz grains were deformed by fan-shaped micro-fractures under compaction, later filled by goethite (Figure 5k).

FIGURE 5 Microfacies of the pre-Late Albian detrital sedimentary rocks of the Demerara Plateau. (a) F1. Cross-bedded calcareous sandstone fragment (DRA-A1-5). (b) F1. Truncated ooid (DRA-A1-7), reflected light. (c) F1. Bivalve shell and micrite (DRA-A1-17), polarised light. (d) F1. Echinoderm fragment (DRA-A1-17), polarised light. E: F1. Mud clast (DRA-A1-17), polarised light. (f) F1. Bivalve shell punched by quartz grains (DRA-A1-17), polarised light. (g) F1. Ooid punched by quartz grains with isopachous calcite cement (DRA-A1-17), polarised light. (h) F2. Calcareous sandstone with bivalve shells, echinoderms and micrite matrix (DRA-B1-14), polarised light. (i) F2. Matrix-filled burrow (DRA-B1-2), polarised light. (j) F3. Quartz-cemented sandstone (DRA-F1-8), polarised-analysed light. The arrow points microstylolite contact between two quartz grains. (k) F4. Ferruginous sandstone (DRA-B1-1), polarised light. The arrow points fan-shaped micro-fractures filled with goethite cement. (l) F5. Shale with iron oxide polyframboids (DRA-B1-25), polarised light. (m–o) F5. Iron oxide polyframboids and framboids (DRA-B1-25) observed with SEM under the backscattered electron beam, and EDS spectrum.

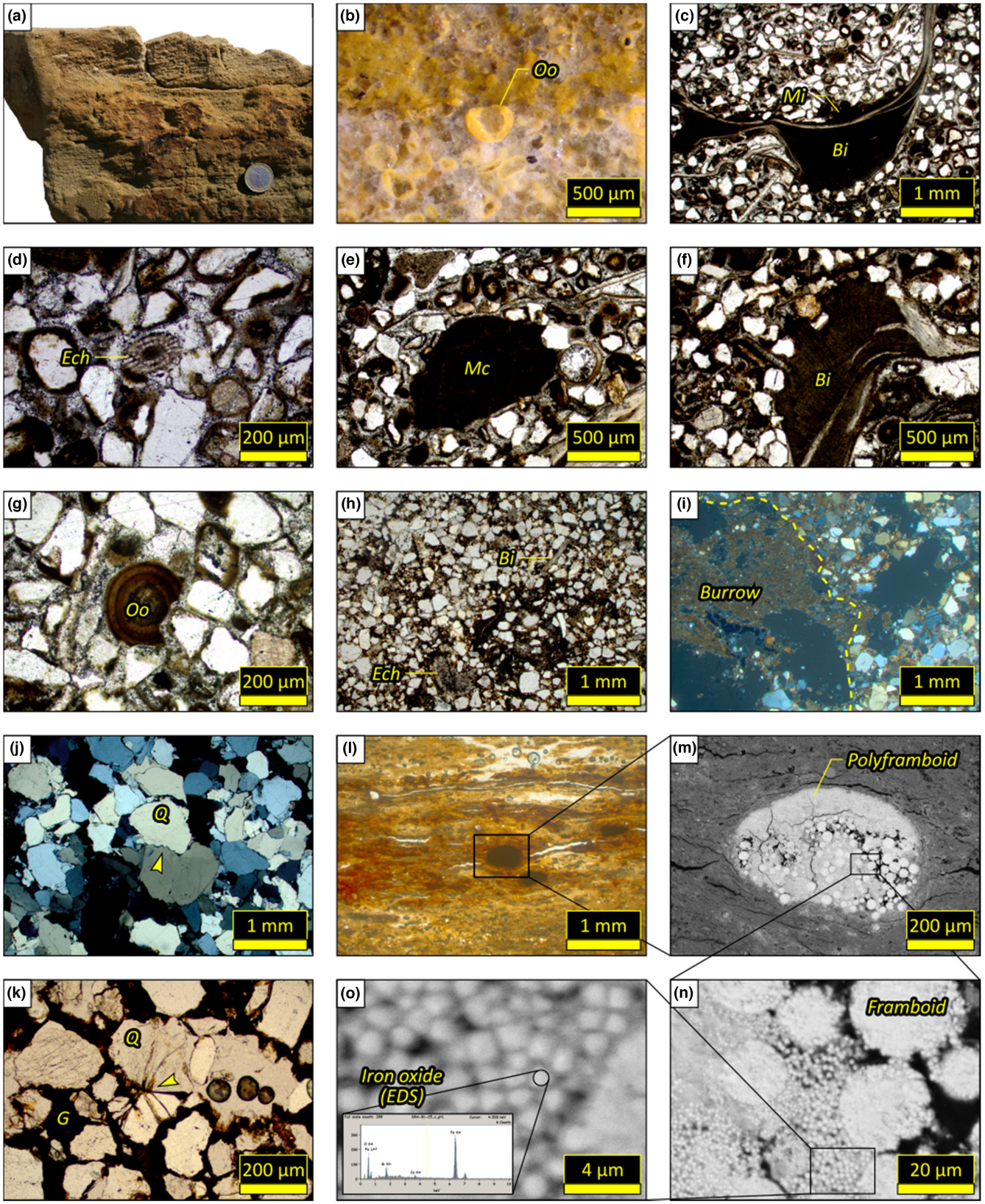

The depositional environment is uncertain. Goethite cement and quartz corrosion indicate that this sample underwent subaerial weathering under an equatorial climate (Garzanti et al., 2013) before drowning. This suggests that it was originally laying under one of the Early Cretaceous erosional unconformities such as Uc6, for which subaerial erosion is documented in industrial wells (Casson et al., 2021).

5.1.5 | Facies 5: shale

This facies occurs in one sample from the DRA-B1 dredge (DRA-B1-25). This sample consists of a laminated shale fragment with sparse quartz grains (up to 50 μm) and polyframboids composed of smaller iron oxide framboids (Figure 5l–o). These framboids are interpreted as pseudomorphs of pyrite framboids. Pyrite framboids precipitate in anoxic environments (Sawlowicz, 2000). These characteristics indicate that this microfacies are deposited in a low-energy environment, such as the offshore zone of an epicontinental sea.

5.2 | Cooling ages

Apatite apparent cooling ages are reported in Table 2. However, considering the limited number of grains (8 and 3, respectively), these ages are not likely representative of the actual cooling age distribution.

Zircon apparent cooling ages range from 58 to 2108 Ma for DRA-A1-6, 71 to 2305 Ma for DRA-B1-3 and 51 to 4617 Ma for DRA-F1-1 (Table 2). The populations of zircon cooling ages in each sample fail the χ^2 homogeneity test and present dispersions of 43%–44%. Best-fitting cooling peak ages were determined using the automatic mixture model of RadialPlotter. Two peaks were obtained for DRA-A1-6 at 170 ± 12 Ma and 382 ± 31 Ma, three peaks for DRA-B1-3 at 127 ± 11, 248 ± 16 and 778 ± 194 Ma and three peaks for DRA-F1-1 at 106 ± 8, 221 ± 12 and 3587 ± 2634 Ma (Figure 6). The distribution of the zircon cooling ages suggests minimum cooling ages as 144 ± 14 Ma for DRA-A1-6, 128 ± 11 Ma for DRA-B1-3 and 105 ± 8 Ma for DRA-F1-1. Cooling ages of detrital zircon are reported with their 2σ error in Table S1.

5.3 | Crystallisation ages

Zircon crystallisation ages are reported in Table S2. Following previous authors (Baesso et al., 2021; Markwitz et al., 2017; Olierook et al., 2019; Philipp et al., 2021; Wang et al., 2021), ages with discordance >10% were discarded (n = 17). We used the $^{206}Pb/^{238}U$ age to date the zircons younger than 1.3 Ga and the $^{206}Pb/^{207}Pb$ age for the zircons older than 1.2 Ga, in agreement with Gehrels et al. (2008). Crystallisation ages range from 564 ± 17 to 2926 ± 53 Ma in DRA-A1-6, 594 ± 17 to 2808 ± 50 Ma in DRA-B1-3 and 452 ± 14 to 2557 ± 57 Ma in DRA-F1-1. Each sample presents a main mode between 600 and 700 Ma. This time interval overlaps 53% of the total population, including 51% of the grains with cooling ages younger than 200 Ma. A less prominent mode occurs between 2.0 and 2.5 Ga (Figure 7).

6 | DISCUSSION

6.1 | Depositional ages

Before discussing the provenance of the detrital material, it is necessary to assess its depositional age and the significance of the detrital zircon apparent cooling ages.

Interpreting the detrital zircon apparent cooling ages requires, as a first step, to bound the depositional age based on independent evidence (Brandon et al., 1998). Because the samples were obtained by dredging, their stratigraphic position is not known a priori. Only one sample (DRA-B1-5) yielded a direct biostratigraphic evidence, the presence of the pollen genus *Afropollis*, suggesting a Late Barremian-Middle Cenomanian age (Moullade et al., 1998). Concerning the other samples, we are left with two types of indirect evidence: the position of the dredge on the seismic line, and the depositional environment. According to previous interpretations of the seismic lines (Loncke et al., 2022; Museur et al., 2021), the samples were collected below the Late Albian unconformity, and one dredge set (DRA-F1) can be ascribed to Unit E (Figure 3c). On the other hand, the microfacies analysis indicates that the three samples deposited in high-energy, shallow environments, hence before the Late Albian drowning of the plateau and the onset of pelagic sedimentation. The DRA-A1 and DRA-B1 samples were deposited in shoreface environments (Facies 1 and 2) such as those documented by the Demerara A2-1 well in Unit D and Unit E (Casson et al., 2021). Facies 3 (DRA-F1 samples) is more difficult to interpret because it is apparently devoid of fossil content. This facies could correspond to the coarse deltaic sandstones of the Stabroek Formation (Unit E) penetrated by the FG2-1 borehole (Casson et al., 2021).

The two sets of evidence (seismic data and depositional environments) consistently point a Late Albian age as a minimal depositional age. We have seen that the population of zircon cooling ages in each sample fails the χ2 homogeneity test. This indicates that the fission tracks did not experience strong annealing due to post-burial heating (Brandon et al., 1998). In addition, none of the minimal cooling ages is strictly younger than Late Albian (Figure 6), which is the minimal depositional age of the samples. The apparent cooling ages can therefore be interpreted as inherited from the sediment source (Bernet & Garver, 2005; Galbraith, 2005; Galbraith & Laslett, 1993; Garver & Brandon, 1994; Vermeesch, 2019), in consistency with the indirect stratigraphic evidence. Considering this hypothesis, the minimal cooling ages provide in turn a lower bound for the depositional ages. DRA-A1-6 is therefore interpreted as younger than 144 ± 14 Ma (Berriasian), DRA-B1-3 as

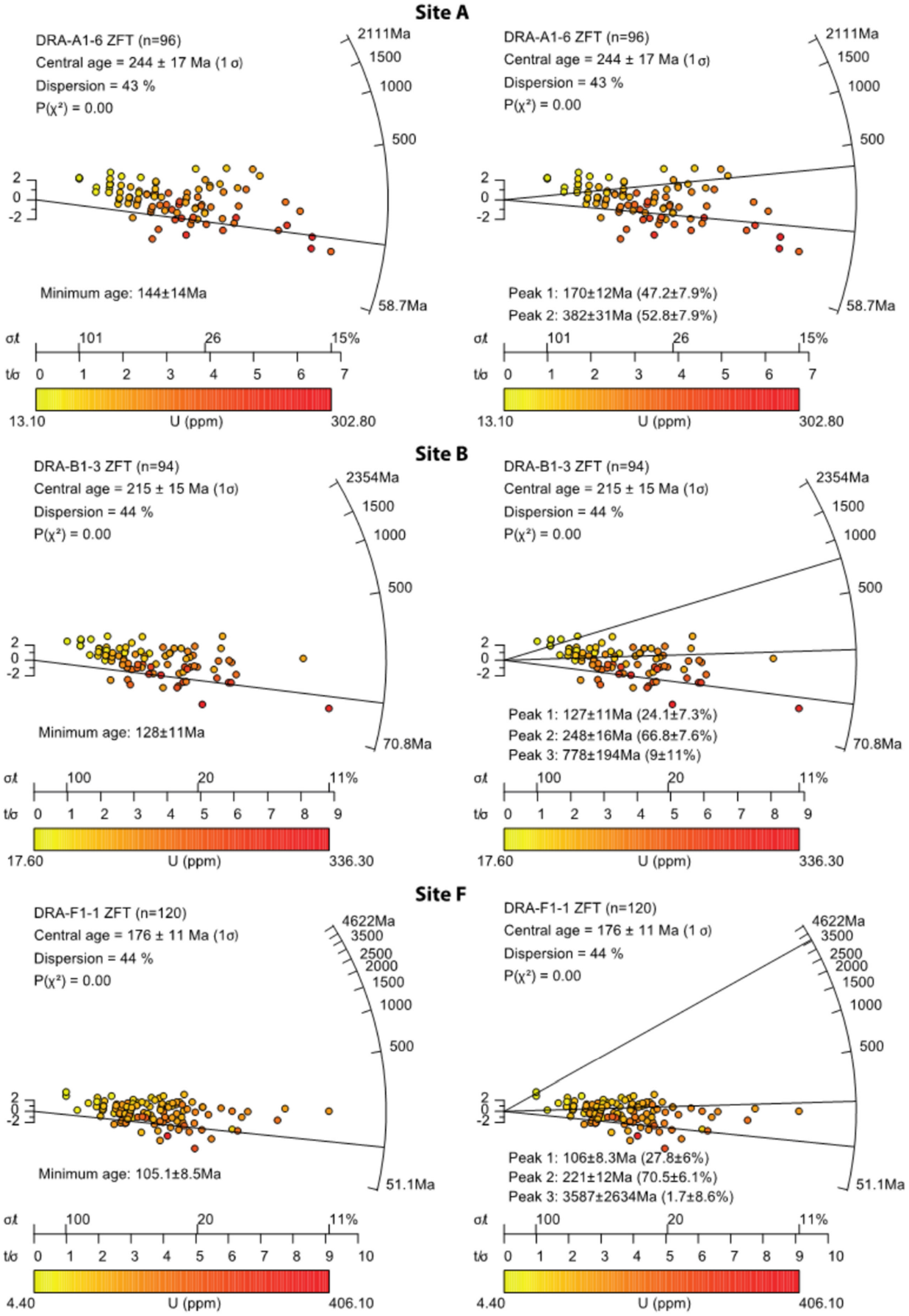

FIGURE 6 Radial plots of detrital zircon fission-track cooling ages from DRA-A1-6 (site A), DRA-B1-3 (site B) and DRA-F1-1 (site F).

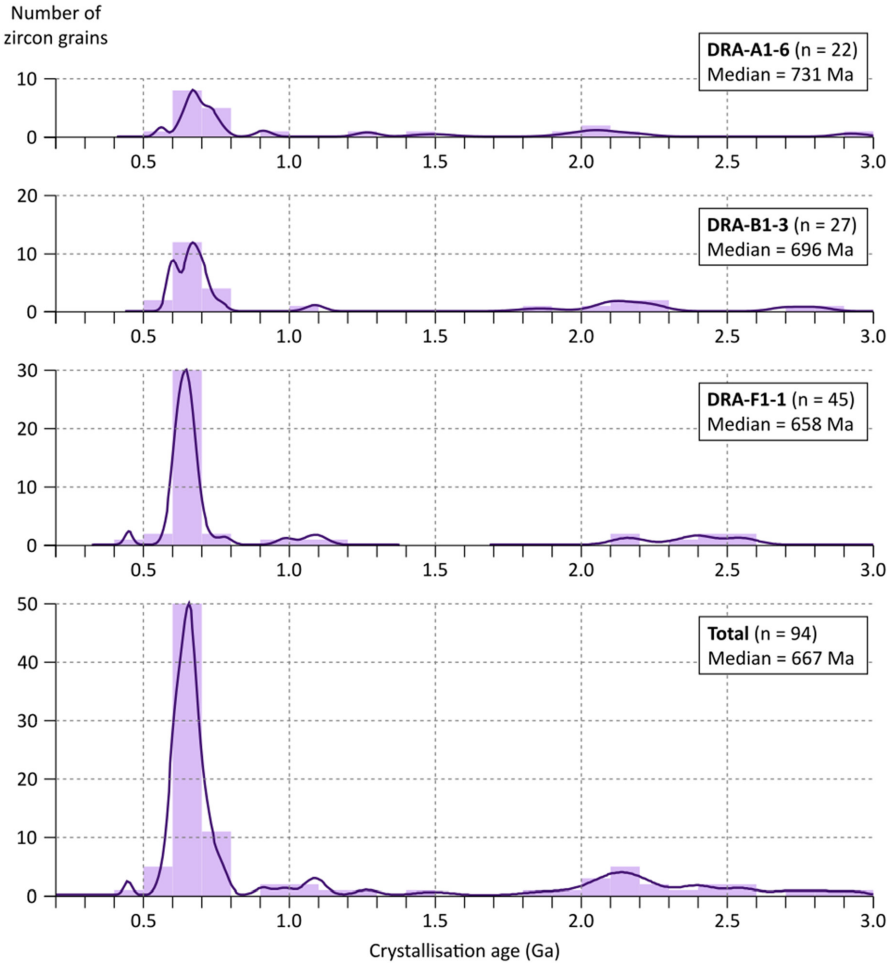

FIGURE 7 Probability density function and histogram of the concordant U–Pb crystallisation ages of detrital zircons from DRA-A1-6 (site A), DRA-B1-3 (site B) and DRA-F1-1 (site F).

younger than 128 ± 11 Ma (Barremian) and DRA-F1-1 as younger than 105 ± 8 Ma (Albian).

6.2 | Source orogens

The three samples present similar distributions of zircon crystallisation ages, with a Palaeoproterozoic peak at 2.0–2.5 Ga and a more prominent Neoproterozoic peak at 600–700 Ma. Detrital zircons from the Cretaceous deposits of the Potiguar basin, north-eastern Brasil, previously yielded a similar distribution of crystallisation ages with two Palaeoproterozoic peaks at 1.7–1.9 Ga and 2.0–2.2 Ga, and a Neoproterozoic peak at 620–550 Ma (Baesso et al., 2021). The Palaeoproterozoic peaks coincide with the Eburnean-Transamazonian orogeny, ca. 2.3–1.8 Ga (Delor et al., 2003; Grenholm et al., 2019; Théveniaut et al., 2006; Vanderhaeghe et al., 1998; Zhao et al., 2002), while the Neoproterozoic peaks overlap the Brasiliano-Pan-African orogeny, ca. 800–500 Ma (Brito Neves et al., 2014; Brito Neves & Cordani, 1991; Villeneuve et al., 2010). The detrital material is therefore interpreted as a mixture of eroded Eburnean-Transamazonian and Pan-African-Brasiliano material.

The Eburnean-Transamazonian orogen extends on both sides of the Equatorial Atlantic Ocean. In Africa, remnants of the Eburnean orogeny occur in the Man-Leo shield, southern West African craton, as the Birimian orogenic belt (Liberia, Ivory Coast and Ghana; Aidoo et al., 2021; Grenholm et al., 2019). In South America, remnants of the Transamazonian orogeny occur as plutonic and metamorphic belts that compose most of the Guiana shield, notably the outcropping basement of onshore Suriname and French Guiana (Delor et al., 2003; Théveniaut et al., 2006; Vanderhaeghe et al., 1998).

The Pan-African-Brasiliano orogeny resulted from the collision of the Archaean-Palaeoproterozoic cratons of Africa and South America during the Neoproterozoic and formed a continuous orogen extending on both continents (Figure 8a), now partially buried under the Amazon basin and the Equatorial Atlantic continental margin deposits (Villeneuve & Marcaillou, 2013; Figure 8b). The Pan-African-Brasiliano orogeny occurred diachronously as successive pulses of magmatic and metamorphic activity.

In South America, remnants of the Brasiliano orogeny occur in the Borborema Province, north-eastern Brazil (Figure 1d) as magmatic arcs dated at 665 ± 5 to 591 ± 8 Ma (Arthaud et al., 2008; dos Santos et al., 2008;

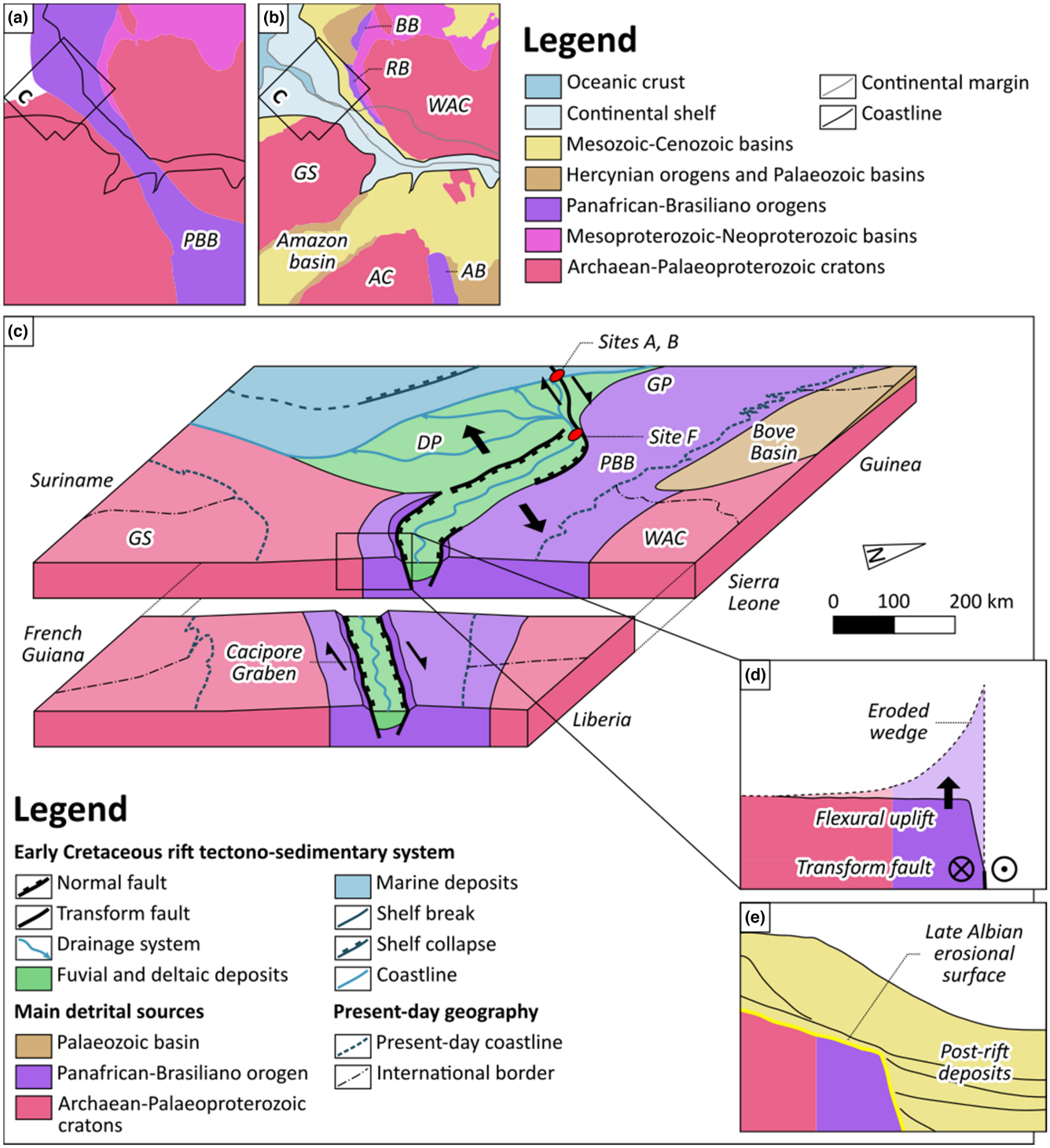

FIGURE 8 Tectono-sedimentary model for the Equatorial Atlantic rifting on the Demerara Plateau-Guinea Plateau conjugate margins. (a) Palaeogeographical reconstruction of the pre-rift basement. Modified from Villeneuve and Marcaillou (2013). (b) Pre-drift palaeogeographical reconstruction with present-day geology. Geological data from Thiéblemont et al. (2016) for Africa and Gómez et al. (2019) for South America. (c) Palaeogeographical reconstruction of the Demerara Plateau and Equatorial Atlantic rift during Aptian. Oblique view from the southeast. Adapted from Casson et al. (2021), in addition to the reconstruction of offshore basements. The offshore extent of the Pan-African-Brasiliano orogen is hypothetical, based on combined evidence from U–Pb dating and fission-track thermochronology of the detrital zircons from the Demerara Plateau. (d) Schematic, hypothetical cross-section of the French Guiana transform rift shoulder during the Equatorial Atlantic rifting. Adapted from Basile and Allemand (2002). E: Schematic, hypothetical cross-section of the post-rift French Guiana transform margin. Legend: cf. Figure 1. DP: Demerara Plateau; GP: Guinea Plateau; GS: Guiana shield; AC: Amazonian Craton; WAC: West African craton; PBB: Pan-African-Brasiliano belt; BB: Bassaride belt; AB: Araguaia belt; RB: Rockelide belt.

Fetter et al., 2003), and on the eastern rim of the Amazonian craton as the Araguaia fold belt (Figure 8b), with granitic veins dated at 583 ± 39 to 498 ± 19 Ma (Moura & Gaudette, 1993). In addition, detrital zircons from the Seridó basin, in the Borborema province, recorded a major orogenic phase at ca. 650 Ma (Van Schmus et al., 2003). Its African counterpart, the Pan-African orogeny, took place at the eastern and western rims of the West African craton. At the eastern rim, the Pan-African orogen occurs as the Dahomeyide fold belt (Ghana, Togo, Benin and Nigeria; Figure 1d), with a magmatic arc dated at 666 ± 16 to 547 ± 15 Ma and associated metamorphic events dated at 704 ± 34 to 548 ± 24 Ma (Kalsbeek et al., 2012). At the western rim, the Pan-African orogen outcrops as the Bassaride and Rockelide fold belts (Figure 8b). In the Bassaride belt (northern Guinea), the peak of magmatic and metamorphic activity is dated at ca. 650 Ma ('Pan-African I event'). In contrast, in the Rockelide fold belt (Guinea, Sierra Leone and Liberia), the Pan-African I event is mostly overprinted by the ca. 550 Ma old 'Pan-African II event' (Brinckmann & Meinhold, 2007; Dallmeyer et al., 1987; Villeneuve et al., 2010; Villeneuve & Cornée, 1994). Hence, the Rockelide fold belt is unlikely to represent the main source of Early Cretaceous detrital material on the Demerara Plateau, although it is the closest presently outcropping Pan-African-Brasiliano orogen according to pre-drift palaeogeographical reconstructions (Figure 8b). The distribution of the zircon crystallisation ages rather suggests that the main source orogen did not undergo significant magmatic and metamorphic activity following the Pan-African I event.

6.3 | Thermal history of the sediment sources

As discussed, statistical and chronological evidence support the interpretation of the zircon cooling ages as mostly inherited from the sediment sources. The main peak ages are therefore expected to date the cooling of the source material.

Archaean-Proterozoic peaks in DRA-F1-1 and DRA-B1-3 are supported by less than 10% of the zircon grain population. In addition, each sample presents two main peaks. The oldest peak is the most prominent, representing ca. 70% of the total population in DRA-B1-3 and DRA-F1-1 and ca. 50% in DRA-A1-6 (Figure 6). In DRA-A-6, this peak occurs at 382 ± 31, after the collapse of the Pan-African-Brasiliano fold belts (Figure 8a) and before the Central Atlantic rifting (Dias et al., 2017). Precambrian gneisses from the Araguaia fold belt (Figure 8b) previously yielded similar peak ages (331 ± 8 to 345 ± 13 Ma) attributed to the Gondwanides orogeny, which took place in the western margin of Gondwana during the Carboniferous (Dias et al., 2017). In DRA-B1-3 and DRA-F1-1, this peak occurs during the Triassic (248 ± 16 and 221 ± 12 Ma, respectively). These ages pre-date the formation of the CAMP but could reflect crustal exhumation during the early phase of Central Atlantic rifting (Loparev et al., 2021).

The youngest peak represents ca. 50% of the zircon grain population in DRA-A1-6 and ca. 25% in DRA-B1-3 and DRA-F1-1 (Figure 6). In DRA-A1-6, this peak fits remarkably well with the age of the magmatic material outcropping on the northern margin of the plateau, 173 ± 2 Ma (Basile et al., 2020). Recent thermochronological evidence from apatite and zircon U-Th/He dating and apatite fission-track analysis indicate that the onshore basement of French Guiana was heated to ca. 100°C between 210 and 140 Ma (Derycke et al., 2021). Crustal heating may have been initiated by the formation of the CAMP, ca. 201 Ma (Marzoli et al., 1999; Marzoli et al., 2018), and may have lasted until continental break-up due to the hotspot activity. The peak of zircon cooling ages at 170 ± 2 Ma therefore reflects the subsequent cooling of the source material.

The two other samples (DRA-B1-3 and DRA-F1-1) present an Early Cretaceous peak at 127 ± 11 and 106 ± 8 Ma, respectively. These ages are very close to the minimal depositional age of the samples, inferred as Late Albian. Considering their 2σ uncertainties, they! overlap with the timing of the Equatorial Atlantic rifting, between ca. 129 and ca. 114 Ma (Basile et al., 1998; Basile et al., 2005; Moulin et al., 2010). During rifting, thermal uplift along the border faults causes denudation of rift shoulders (Withjack et al., 2002). Indeed, Derycke et al. (2021) previously documented on the offshore basement of French Guiana a cooling of ca. 60°C between 140 and 90 Ma, attributed to the Equatorial Atlantic rifting. Considering a thermal gradient of 30°C km^{-1}, such cooling represents an uplift of 2 km. By contrast, the detrital zircons from the Demerara Plateau recorded a cooling of at least 240°C, implying an uplift of 8 km for a similar thermal gradient. This represents a maximal uplift, considering that the thermal gradient could have been higher due to volcanic activity such as documented during the Aptian-Albian on the Guinea Plateau (Olyphant et al., 2017). Yet, this observation raises the following problem: what mechanism is able to bring in a few million years only rocks that were initially at temperatures of >240°C up to the surface, before erosion and sedimentation? Along transform margins, the difference in thickness between the continental and the oceanic crusts brought in contact by strike-slip displacement promotes the erosion of the rift shoulder. As a result, the rift shoulder is subject to intense flexural uplift by isostatic compensation as long as the transform

fault remains active (Figure 8d). Previous works suggest that flexural uplift along transform margins can cause erosion of a total thickness of several kilometres (Basile & Allemand, 2002). The uplift is limited to the first 20–50 km of the margin, starting from the transform fault. This suggests that the exhumation of the zircons occurred on a transform margin during the Early Cretaceous rifting.

6.4 | Source-to-sink model

The distribution of the detrital zircon crystallisation ages indicates that the sediment source was either a Neoproterozoic basin contemporary with the Pan-African-Brasiliano orogeny, such as the Seridó basin (Van Schmus et al., 2003), or the orogen itself. The latter hypothesis is the most likely, considering the relative abundance of Pan-African-Brasiliano zircons (more than half of the population). In addition, the thermal history of the zircons points to an Equatorial Atlantic transform margin as the source area. Locating the source area therefore requires to propose a source-to-sink model matching with these evidence.

On the northern margin of the Demerara Plateau, the Precambrian basement (Unit A) is presently overlain by the Jurassic syn-rift unit (Unit B). It was therefore not eroded during the Early Cretaceous rifting. This is also the case on the southern margin of the Guinea Plateau (Loncke et al., 2022; Mercier de Lépinay, 2016). This transform segment formed on a former Central Atlantic divergent margin. Hence, the continental crust was previously thinned during Central Atlantic rifting, and one can assume that the flexural uplift during the Early Cretaceous transform phase was insufficient to erode the margin down to the Precambrian basement.

The French Guiana hyper-oblique margin (Figure 1b) represents a more plausible source area. Unlike the northern margin of the Demerara Plateau, the French Guiana hyper-oblique margin accommodated the shear movement during the Equatorial Atlantic rifting with a series of smaller-scale transfer zones (Sapin et al., 2016) forming an oblique rift basin, the Cacipore graben (Figure 8c). At the intersection between the eastern divergent margin of the Demerara Plateau and the French Guiana margin, seismic data indicate that Unit A is directly overlain by the Early Cretaceous syn-rift deposits (Unit E; Basile et al., 2022; Graindorge et al., 2022; Loncke et al., 2022; Museur et al., 2021; Sapin et al., 2016). This implies that the rift shoulder was eroded down to the Precambrian basement along the French Guiana margin, during the early phase of Equatorial Atlantic rifting.

Casson et al. (2021) previously suspected that the Cacipore graben axis funnelled the syn-rift detrital inputs to the Demerara Plateau. This hypothesis matches well with the thermal history of the zircons. Indeed, the former catchment area of the Cacipore graben was delimited by the rift shoulders. Hence, the sediments produced by the erosion of the transform scarps were collected by the graben drainage system. At that time, shallow marine sedimentation occurred on the Demerara Plateau (Casson et al., 2021; Loncke et al., 2022; Mercier de Lépinay, 2016), which therefore represented the outlet of the drainage system (Figure 8c).

This source-to-sink model postulates that the Precambrian basement of the French Guiana margin and eastern Demerara Plateau are composed of Pan-African-Brasiliano orogenic material, instead of the Guyana Shield as proposed by Mercier de Lépinay (2016). Testing this hypothesis would necessitate sampling and dating the basement of the French Guiana transform margin, which presently lies under 2 km of post-rift deposits. Yet, our model supports earlier works of Villeneuve et al. (1993), who proposed that the Equatorial Atlantic rift took place along the former Pan-African lineaments.

7 | CONCLUSION

Provenance analysis of the sandstones dredged on the northern margin of the Demerara Plateau brings new insights into the tectono-sedimentary setting of the Equatorial Atlantic rifting. The examination of the results of microfacies analysis, zircon fission-track analysis, zircon U–Pb dating, combined with existing seismic and stratigraphic data, shed light on the sediment history from source to sink. The detrital material is mostly derived from a 650 Myr old Pan-African-Brasiliano orogen, presently buried under the French Guiana continental margin. The detrital zircons recorded several cooling phases attesting to the complex thermal history of the source material. Three main cooling phases were recognised during the Mesozoic. The first one occurred during the Triassic, presumably in response to exhumation during the early phase of the Central Atlantic rifting. The second took place during the Middle Jurassic, ca. 170 Ma in the aftermath of a peak of magmatic activity previously attributed to the Sierra Leone hotspot. The last cooling phase (127 ± 11 and 106 ± 8 Ma) occurred during the Equatorial Atlantic rifting as a result of flexural uplift along the French Guiana hyper-oblique margin. The eroded material was funnelled via the Cacipore graben and ultimately sustained syn-rift detrital sedimentation on the Demerara Plateau.

ACKNOWLEDGEMENTS

We gratefully thank the crew of French oceanographic research vessel *Pourquoi pas ?* for the organisation of

onboard operations, and Nathaniel Findling, from the Institute of Earth Sciences (ISTerre), Université Grenoble Alpes, France, for monitoring the XRD analyses and quantifying the mineral phases. The work of I. Girault was funded by an internship grant from the University of Burgundy, Dijon, France, with the support of Michel Guiraud. We thank Max Casson and Alexis Derycke for their helpful review. We wish to dedicate this article to the memory of Jean-Louis Paquette, cherished by his friends and respected by his colleagues for his research.

CONFLICT OF INTEREST STATEMENT

We wish to confirm that there are no known conflicts of interest associated with this publication and there has been no significant financial support for this work that could have influenced its outcome.

PEER REVIEW

The peer review history for this article is available at https://publons.com/publon/10.1111/bre.12758.

DATA AVAILABILITY STATEMENT

The data that support the findings of this study are available in the supplementary material of this article.

ORCID

Igor Girault https://orcid.org/0000-0002-9893-8843
Matthias Bernet https://orcid.org/0000-0001-5046-7520
Arnauld Heuret https://orcid.org/0000-0003-0186-5260

REFERENCES

Aidoo, F., Nude, P., Sun, F.-Y., Li, Z.-X., Liang, T., & Zhang, S.-B. (2021). Paleoproterozoic transitional TTG-like metagranites from the Dahomeyide Belt, Ghana: Constraints on the evolution of the Birimian-Eburnean Orogeny. *Precambrian Research*, *353*, 106024.

Amante, C., & Eakins, B. W. (2009). *ETOPO1 1 arc-minute global relief model: Procedures, data sources and analysis. NOAA technical memorandum NESDIS NGDC-24.* National Geophysical Data Center, NOAA.

Arthaud, M., Caby, R., Fuck, R., Dantas, E., & Parente, C. (2008). Geology of northern Borborema Province, NE Brazil and its correlation with Nigeria, NW Africa. *Geological Society, London, Special Publications*, *294*, 49–67.

Baesso, A., Remus, M. V. D., Pereira, B. R. B., Alkmim, A. R., Lana, C. C., Vignol-Lelarge, M. L., & Porcher, C. C. (2021). Insights into sedimentary provenance and the evolution of the Potiguar Basin, NE Brazil, using U-Pb ages and Lu-Hf isotopes in detrital zircons. *Marine and Petroleum Geology*, *131*, 105170.

Basile, C., & Allemand, P. (2002). Erosion and flexural uplift along transform faults. *Geophysical Journal International*, *151*, 646–653.

Basile, C., Girault, I., Heuret, A., Loncke, L., & Poetisi, E. (2016). *Campagne DRADEM – Juillet 2016 – Rapport scientifique* (p. 47). (Research report). ISTerre, CNRS UMR 5275, Université Grenoble- Alpes.

Basile, C., Girault, I., Paquette, J. L., Agranier, A., Loncke, L., Heuret, A., & Poetisi, E. (2020). The Jurassic magmatism of the Demerara Plateau (offshore French Guiana) as a remnant of the Sierra Leone hotspot during the Atlantic rifting. *Scientific Reports*, *10*, 7486.

Basile, C., Loncke, W. R., Graindorge, D., Klingelhoefer, F., Museur, T., Heuret, A., Lesourd-Laux, T., & Vetel, W. (2022). Initiation of transform continental margins: The example of the demerara plateau. The. *Geological Society Special Publications*, *524*.

Basile, C., Maillard, A., Patriat, M., Gaullier, V., Loncke, L., Roest, W., Mercier de Lépinay, M., & Pattier, F. (2013). Structure and evolution of the Demerara Plateau, offshore French Guiana: Rifting, tectonic inversion and post-rift tilting at transform–divergent margins intersection. *Tectonophysics*, *591*, 16–29.

Basile, C., Mascle, J., Benkhelil, J., & Bouillin, J.-P. (1998). Geodynamic evolution of the Côte D'ivoire-Ghana transform margin: An overview of leg 159 results. In J. Mascle, G. P. Lohmann, & M. Moullade (Eds.), *Proceedings of the ocean drilling program. Scientific Results* (Vol. *159*, pp. 101–110).

Basile, C., Mascle, J., & Guiraud, R. (2005). Phanerozoic geological evolution of the equatorial Atlantic. *Journal of African Earth Sciences*, *43*, 275–282.

Benkhelil, J., Mascle, J., & Tricart, P. (1995). The Guinea continental margin: An example of a structurally complex transform margin. *Tectonophysics*, *248*, 117–137.

Bernet, M., Brandon, M., Garver, J., Balestrieri, M. L., Ventura, B., & Zattin, M. (2009). Exhuming the Alps through times: Clues from detrital zircon fission-track thermochronology. *Basin Research*, *21*(6), 781–798.

Bernet, M., & Garver, J. I. (2005). Fission-track analysis on detrital zircon. *Reviews in Mineralogy and Geochemistry*, *58*, 205–238.

Boggs, S., Jr. (2009). *Petrology of sedimentary rocks* (2nd ed., p. 600). Cambridge University Press.

Brandon, M. T., Roden-Tice, M. K., & Garver, J. I. (1998). Late Cenozoic exhumation of the Cascadia accretionary wedge in the Olympic Mountains, northwest Washington State. *Geological Society of America Bulletin*, *110*, 985–1009.

Brinckmann, J., Meinhold, K.D., 2007. La géologie de la chaîne des Bassarides et des terrains environnants au Nord-Ouest de la Guinée. Geol. Jahr., Hannover, B (Vol. *SB1*, p. 446).

Brito Neves, B. B., & Cordani, U. G. (1991). Tectonic evolution of South America during the Late Proterozoic. *Precambrian Research*, *53*, 23–40.

Brito Neves, B. B., Fuck, R., & Pimentel, M. (2014). The Brasiliano collage in South America: A review. *Brazilian Journal of Geology*, *44*, 493–518.

Brunet, M., Dejax, J., Brillanceau, A., Congleton, J., Downs, W., Duperon-Laudoueneix, M., Eisenmann, V., Flanagan, K., Flynn, L., Heintz, E., Hell, J., Jacobs, L., Jehenne, Y., Ndjeng, E., Mouchelin, G., & Pilbeam, D. (1988). Mise en évidence d'une sédimentation précoce d'âge Barrémien dans le fossé de la Bénoué en Afrique occidentale (Bassin du Mayo Oulo Léré, Cameroun), en relation avec l'ouverture de l'Atlantique sud. *Comptes rendus de l'Académie des Sciences*, *306*, 1125–1130.

Casson, M., Jeremiah, J., Calvès, G., de Ville de Goyet, F., Reuber, K., Bidgood, M., Rehakova, D., Bulot, L., & Redfern, J. (2021). Evaluating the segmented post-riftstratigraphic architecture of the guyanas continental margin. *Petroleum Geoscience*, *27*(3).

Dallmeyer, R. D., Caen-Vachette, M., & Villeneuve, M. (1987). Emplacement age of post-tectonic granites in southern

Guinea (West Africa) and the peninsular Florida subsurface: Implications for origins of southern Appalachian exotic terranes. *Geological Society of America Bulletin*, *99*, 87–93.

Delor, C., de Roever, E. W. F., Lafon, J.-M., Lahondère, D., Rossi, P., Cocherie, A., Guerrot, C., & Potrel, A. (2003). The Bakhuis ultrahigh-temperature granulite belt (Suriname): II. Implications for late Transamazonian crustal stretching in a revised Guiana shield framework. *Géologie de la France*, *2-3-4*, 207–230.

Derycke, A., Gautheron, C., Barbarand, J., Bourbon, P., Aetgeerts, G., Simon-Labric, T., Sarda, P., Pinna-Jamme, R., Boukari, C., & Haurine, F. (2021). French Guiana margin evolution: From Gondwana break-up to Atlantic opening. *Terra Nova*, *33*, 415–422.

Dias, A., Moura, C., Milhomem Neto, J., Chemale, F., Jr., Girelli, T., & Masuyama, K. M. (2017). Geochronology and thermochronology of the gneisses of the Brasiliano/Pan-African Araguaia Belt: Records of exhumation of West Gondwana and Pangea break up. *Journal of South American Earth Sciences*, *80*, 174–191.

Dodson, M. H. (1973). Closure temperature in cooling geochronological and petrological systems. *Contributions to Mineralogy and Petrology*, *40*, 259–274.

dos Santos, T. J. S., Fetter, A. H., & Neto, J. A. N. (2008). Comparisons between the northwestern Borborema Province, NE Brazil, and the southwestern Pharusian Dahomey Belt, SW Central Africa. *Geological Society, London, Special Publications*, *294*, 101–119.

Erbacher, J., Mosher, D. C., Malone, M. J., Sexton, P., & Wilson, P. A. (2004). Proceedings of the ocean drilling program, initial reports. Vol. 207. Demerera rise: Equatorial cretaceous and Paleogene paleoceanographic transect, Western Australia. Covering Leg 207 of the cruises of the Drilling Vessel "Joides Resolution", Bridgetown, Barbados, to Rio de Janeiro, Brazil, Sites 1257-1261, 11 January-6 March 2003. Texas A & M University Ocean Drilling Program.

Fanget, A. S., Loncke, L., Pattier, F., Marsset, T., Roest, W. R., Tallobre, C., de Madron, X. D., & Hernandez-Molina, F. J. (2020). A synthesis of the sedimentary evolution of the Demerara Plateau (Central Atlantic Ocean) from the late Albian to the Holocene. *Marine and Petroleum Geology*, *114*(3), 104195.

Fetter, A. H., Saraiva dos Santos, T. J., Van Schmus, W. R., Hackspacher, P. C., Brito Neves, B. B., Arthaud, M. H., Nogueira Neto, J. A., & Wernick, E. (2003). Evidence for Neoproterozoic continental arc magmatism in the Santa Quitéria batholith of Ceara State, NW Borborema Province, NE Brazil: Implications for the assembly of West Gondwana. *Gondwana Research*, *6*(2), 265–273.

Flügel, E. (2009). Microfacies of carbonate rocks. In *Analysis, interpretation and application* (2nd ed., p. 984). Springer.

Fox, P. J., Heezen, B. C., & Johnson, G. L. (1970). Jurassic sandstone from the tropical Atlantic. *Science*, *170*, 1402–1404.

Galbraith, R. F., & Green, P. F. (1990). Estimating the component ages in a finite mixture. *Nuclear Tracks and Radiation Measurements*, *17*, 197–206.

Galbraith, R. F., & Laslett, G. M. (1993). Statistical models for mixed fission-track ages. *Nuclear Tracks and Radiation Measurements*, *21*(4), 459–470.

Galbraith, R. G. (2005). *Statistics for fission-track analysis* (p. 240). Chapman & Hall/CRC.

Garver, J. I., & Brandon, M. T. (1994). Fission-track ages of detrital zircons from cretaceous strata, southern British Columbia—Implications for the Baja BC hypothesis. *Tectonics*, *13*(2), 401–420.

Garzanti, E., Padoan, M., Andò, S., Resentini, A., Vezzoli, G., & Lustrino, M. (2013). Weathering and relative durability of detrital minerals in equatorial climate: Sand petrology and geochemistry in the East African Rift. *The Journal of Geology*, *121*, 547–580.

Gehrels, G. E., Valencia, V. A., & Ruiz, J. (2008). Enhanced precision, accuracy, efficiency, and spatial resolution of U-Pb ages by laser ablation–multicollector–inductively coupled plasma–mass spectrometry. *Geochemistry, Geophysics, Geosystems*, *9*, Q03017.

Geoffroy, L. (2005). Volcanic passive margins. *Comptes Rendus Geoscience*, *337*, 1395–1408.

Girault, I. (2017). *Pétrographie et thermochronologie du Plateau de Demerara (Guyane-Suriname)* (p. 41). (Master thesis). Université de Bourgogne.

Gómez, J., Schobbenhaus, C., Montes, N. E., & Compilers. (2019). Geological Map of South America 2019. Scale 1:5 000 000. Commission for the Geological Map of the World (CGMW), Colombian Geological Survey, and Geological Survey of Brazil. Paris.

Gouyet, S. (1988). Evolution tectono-sédimentaire des marges guyanaise et nord brésilienne au cours de l'ouverture de l'Atlantique Sud (PhD Thesis).

Graindorge, D., Museur, T., Klingelhoefer, F., Roest, W. R., Basile, C., Loncke, L., Sapin, F., Heuret, A., Perrot, J., Marcaillou, B., Lebrun, J. F., & Deverchere, J. (2022). Deep structure of the Demerara Plateau and its two-fold tectonic evolution: From a volcanic margin to a transform marginal plateau, insights from the conjugate Guinea plateau. *The Geological Society Special Publications*, *524*.

Greenroyd, C. J., Peirce, C., Rodger, M., Watts, A. B., & Hobbs, R. W. (2008). Demerara Plateau—The structure and evolution of a transform passive margin. *Geophysical Journal International*, *172*, 549–564.

Grenholm, M., Jessell, M., & Thébaud, N. (2019). A geodynamic model for the Paleoproterozoic (ca. 2.27–1.96 Ga) Birimian Orogen of the southern West African Craton—Insights into an evolving accretionary-collisional orogenic system. *Earth Science Reviews*, *192*, 138–193.

Hart, N. R., Stockli, D. S., & Hayman, N. W. (2016). Provenance evolution during progressive rifting and hyperextension using bedrock and detrital zircon U-Pb geochronology, Mauléon Basin, western Pyrenees. *Geosphere*, *12*(4), 1166–1186.

Hayes, D. E., Pimm, A. C., Beckman, J. B., Benson, W. E., Berger, W. H., Roth, P. H., Supko, P. R., & von Rad, U. (1972). *Initial reports of the Deep Sea Drilling Project* (Vol. *14*, p. 975). US government printing office.

Hurai, V., Paquette, J. L., Huraiova, M., & Konecny, P. (2010). U-Th-Pb geochronology of zircon and monazite from syenite and pincinite xenoliths in Pliocene alkali basalts of the intra-Carpathian back-arc basin. *Journal of Volcanology and Geothermal Research*, *198*(3–4), 275–287.

Jackson, S. E., Pearson, N. J., Griffin, W. L., & Belousova, E. A. (2004). The application of laser ablation-inductively coupled plasma-mass spectrometry to in situ U–Pb zircon geochronology. *Chemical Geology*, *211*, 47–69.

Kalsbeek, F., Affaton, P., Ekwueme, B., Frei, R., & Thrane, K. (2012). Geochronology of granitoid and metasedimentary rocks from

Togo and Benin, West Africa: Comparisons with NE Brazil. *Precambrian Research*, *196–197*, 218–233.

Kohn, B., Chung, L., & Gleadow, A. (2019). Fission-track analysis: Field collection, sample preparation and data acquisition. In M. Malusà & P. Fitzgerald (Eds.), *Fission-track Thermochronology and its application to geology* (pp. 25–48). Springer.

Labails, C., Olivet, J.-L., Aslanian, D., & Roest, W. R. (2010). An alternative early opening scenario for the Central Atlantic Ocean. *Eartn and Planetary Science Letters*, *297*, 355–368.

Loncke, L., Maillard, A., Basile, C., Roest, W. R., Bayon, G., Pattier, F., Mercier de Lépinay, M., Grall, C., Droz, L., Marsset, T., Giresse, P., Caprais, J. C., Cathalot, C., Graindorge, D., Heuret, A., Lebrun, J. F., Bermell, S., Marcaillou, B., Bassetti, M.-A., … Bourrin, F. (2016). Structure of the demerara passive transform margin and associated sedimentary processes. Preliminary results from the IGUANES cruise. *Geological Society, London, Special Publications*, *431*, 179–197.

Loncke, L., Mercier de Lépinay, M., Basile, C., Maillard, A., Roest, W. R., de Clarens, P., Patriat, M., Gaullier, V., Klingelhoefer, F., Graindorge, D., & Sapin, F. (2022). Compared structure and evolution of the conjugate Demerara and Guinea transform marginal plateaus. *Tectonophysics*, *822*, 229112.

Loparev, A., Rouby, D., Chardon, D., Dall'Asta, M., Sapin, F., Bajolet, F., Ye, J., & Paquet, F. (2021). Superimposed rifting at the junction of the Central And Equatorial Atlantic: Formation of the passive margin of the Guiana shield. *Tectonics*, *40*, e2020TC006159.

Ludwig, K. R. (2001). *User's manual for Isoplot/Ex Version 2.49, a geochronological toolkit for Microsoft EXCEL* (p. 55). Berkeley Geochronological Center, Special Publication 1a.

Markwitz, V., Kirkland, C. L., Wyrwoll, K.-H., Hancock, E. A., Evans, N. J., & Lu, Y. (2017). Variations in zircon provenance constrain age and geometry of an Early Paleozoic rift in the Pinjarra Orogen, East Gondwana. *Tectonics*, *36*, 2477–2496.

Marzoli, A., Callegaro, S., Dal Corso, J., Davies, J., Chiaradia, M., Youbi, N., Bertrand, H., Reisberg, L., Merle, R., & Jourdan, F. (2018). The Central Atlantic magmatic province (CAMP): A review. In L. Tanner (Ed.), *The Late Triassic World. Topics in geobiology* (Vol. *46*, pp. 91–125). Springer.

Marzoli, A., Renne, P. R., Piccirillo, E. M., Ernesto, M., Bellieni, G., & De Min, A. (1999). Extensive 200-million-year-old continental flood basalts of the Central Atlantic Magmatic Province. *Science*, *284*, 616–618.

Mercier de Lépinay, M. (2016). *Inventaire mondial des marges transformantes et évolution tectonosédimentaire des plateaux de Demerara et de Guinée* (p. 335) (Ph D. Thesis). Université de Perpignan.

Moulin, M., Aslanian, D., & Unternehr, P. (2010). A new starting point for the South and Equatorial Atlantic Ocean. *Earth-Science Reviews*, *98*, 1–37.

Moullade, M., Watkins, D. K., Oboh-Ikuenobe, F. E., Bellier, J.-P., Masure, E., Holbourn, A. E. L., Erbacher, J., Kuhnt, W., Pletsch, T., Kaminski, M. A., Rauscher, R., Shafik, S., Yepes, O., Dejax, J., Gregg, J. M., Shin, I. C., & Schuler, M. (1998). Mesozoic biostratigraphic, paleoenvironmental, and paleobiogeographic synthesis, equatorial Atlantic. *Proceedings of the Ocean Drilling Program, Scientific Results*, *159*, 481–490.

Moura, C., & Gaudette, H. (1993). Evidence of Brasiliano/Pan-African deformation in the Araguaia belt: Implication for Gondwana evolution. *Revista Brasileira de Geociencias*, *23*, 117–123.

Mullen, E. K., Paquette, J. L., Tepper, J. H., & McCallum, I. S. (2018). Temporal and spatial evolution of the Northern Cascade Arc magmatism revealed by LA-ICP-MS U-Pb zircon dating. *Canadian Journal of Earth Sciences*, *55*(5), 443–462.

Museur, T., Graindorge, D., Klingelhoefer, F., Roest, W. R., Basile, C., Loncke, L., & Sapin, F. (2021). Deep structure of the Demerara Plateau: From a volcanic margin to a transform marginal plateau. *Tectonophysics*, *803*, 228645.

Nemčok, M., Rybár, S., Odegard, M. E., Dickson, W., Pelech, O., Ledvenyiova, L., Molčan Matejová, M., Molcan, M., Hermeston, S., Jones, D., Cuervo, E., Cheng, R., & Forero, G. (2015). Development history of the southern terminus of the Central Atlantic; Guyana–Suriname case study. *Geological Society, London, Special Publications*, *431*.

Olierook, H. K. H., Barham, M., Fitzsimons, I. C. W., Timms, N. E., Jiang, Q., Evans, N. J., & McDonald, B. J. (2019). Tectonic controls on sediment provenance evolution in rift basins: Detrital zircon U–Pb and Hf isotope analysis from the Perth Basin, Western Australia. *Gondwana Research*, *66*, 126–142.

Olyphant, J. R., Johnson, R. A., & Hughes, A. N. (2017). Evolution of the Southern Guinea Plateau: Implications on Guinea-Demerara Plateau formation using insights from seismic, subsidence, and gravity data. *Tectonophysics*, *717*, 358–371.

Paquette, J.-L., Piro, J.-L., Devidal, J.-L., Bosse, V., Didier, A., Sannac, S., & Abdelnour, Y. (2014). Sensitivity enhancement in LA-ICP-MS by N2 addition to carrier gas: Application to radiometric dating of U-Th-bearing minerals. *Agilent ICP-MS Journal*, *58*, 4–5.

Philipp, R. P., Pimentel, M. M., Basei, M. A. S., Salvi, M., De Lena, L. O. F., Vedana, L., Gubert, M. L., Lopes, C., Laux, J. H., & Camozzato, E. (2021). U–Pb detrital zircon dating applied to metavolcano-sedimentary complexes of the São Gabriel Terrane: New constraints on the evolution of the Dom Feliciano Belt. *Journal of South American Earth Sciences*, *110*, 103409.

Reiners, P. W., & Brandon, M. T. (2006). Using thermochronology to understand orogenic erosion. *Annual Review of Earth and Planetary Sciences*, *34*, 419–466.

Reuber, K. R., Pindell, J., & Horn, B. W. (2016). Demerara Rise, offshore Suriname: Magma-rich segment of the Central Atlantic Ocean, and conjugate to the Bahamas hot spot. *Interpretation*, *T142*, T141–T155.

Roberts, D.G., Backman, J., Morton, A., Murray, J., Keene, J.B., 1984. Evolution of Volcanic Rifted Margins: Synthesis of Leg 81 Results on the West Margin of Rockall plateau. Initial reports DSDP, Leg 81, Southampton to Azores (Vol. *81*, pp. 883–911).

Sahabi, M., Aslanian, D., & Olivet, J.-L. (2004). Un nouveau point de départ pour l'histoire de l'Atlantique Central. *Comptes Rendus Geosciences*, *33*, 1041–1052.

Sapin, F., Davaux, M., Dall'Asta, M., Lahmi, M., Baudot, G., & Ringenbach, J. C. (2016). Post-rift subsidence of the French Guiana hyper-oblique margin: From rift-inherited subsidence to Amazon deposition effect. *Geological Society, London, Special Publications*, *431*.

Sawlowicz, Z. (2000). Framboids: From their origin to application. *Prace Mineralogiczne*, *88*, 80.

Théveniaut, H., Delor, C., Lafon, J.-M., Monié, P., Rossi, P., & Lahondère, D. (2006). Paleoproterozoic (2155–1970 Ma)

evolution of the Guiana Shield (Transamazonian event) in the light of new paleomagnetic data from French Guiana. *Precambrian Research*, *150*, 221–256.

Thiéblemont, D., Liégeois, J. P., Fernandez-Alonso, M., Le Ouabadi, A., Gall, B., Maury, R., Jalludin, M., Vidal, M. O., Gbélé, C., Tchaméni, R., Michard, A., Nehlig, P., Rossi, P., & Chêne, F. (2016). Geological Map of Africa at 1:10M scale, CGMW-BRGM 2016.

van Achterbergh, E., Griffin, W. L., & Stiefenhofer, J. (2001). Metasomatism in mantle xenoliths from the Letlhakane kimberlites: Estimation of element fluxes. *Contributions to Mineralogy and Petrology*, *141*(4), 397–414.

Van Schmus, W. R., Brito Neves, B. B., Williams, I. S., Hackspacher, P. C., Fetter, A. H., Dantas, E. L., & Babinski, M. (2003). The Seridó Group of NE Brazil, a late Neoproterozoic pre- to syn-collisional basin in West Gondwana: Insights from SHRIMP U–Pb detrital zircon ages and Sm–Nd crustal residence (TDM) ages. *Precambrian Research*, *127*(4), 287–327.

Vanderhaeghe, O., Ledru, P., Thiéblemeont, D., Egal, E., Cocherie, A., Tegyey, M., & Milesi, J. P. (1998). Contrasting mechanism of crustal growth Geodynamic evolution of the granite-greenstone belts of French Guiana. *Precambrian Research*, *85*, 1–25.

Vermeesch, P. (2004). How many grains are needed for a provenance study? *Earth and Planetary Science Letters*, *224*, 441–451.

Vermeesch, P. (2009). RadialPlotter: A Java application for fission track, luminescence and other radial plots. *Radiation Measurements*, *44*(4), 409–410.

Vermeesch, P. (2019). Statistics for fission-track thermochronology. In M. Malusà & P. Fitzgerald (Eds.), *Fission-track thermochronology and its application to geology* (Chapter 6, pp. 109–122). Springer.

Villeneuve, M., & Cornée, J.-J. (1994). Structure, evolution and palaeogeography of the West African Craton and bordering belts during the Neoproterozoic. *Precambrian Research*, *69*, 307–326.

Villeneuve, M., El Archi, A., & Nzamba, J. (2010). Les chaînes de la marge occidentale du Craton Ouest-Africain, modèles géodynamiques. *Comptes Rendus Geoscience*, *342*(1), 1–10.

Villeneuve, M., & Marcaillou, B. (2013). Pre-Mesozoic origin and paleogeography of blocks in the Caribbean, south Appalachian and West African domains and their impact on the post "variscan" evolution. *Bulletin. Société Géologique de France*, *184*(1–2), 5–20.

Villeneuve, M., Rochet, J., & Faye, M. (1993). Pan-African and Hercynian structural inheritance on the West African Atlantic margin (from Mauritania to Liberia). *Bulletin Société Géologique de France*, *164*(6), 851–860.

Wang, J., Wu, C., Jiao, Y., & Yuan, B. (2021). Middle–Late Triassic sedimentary provenance of the southern Junggar Basin and its link with the post-orogenic tectonic evolution of Central Asia. *Scientific Reports*, *11*, 17041.

Wiedenbeck, M., Alle, P., Corfu, F., Griffin, W. L., Meier, M., Oberli, F., Vonquadt, A., Roddick, J. C., & Speigel, W. (1995). 3 natural zircon standards for U-Th-Pb, Lu-Hf, trace-element and REE analyses. *Geostandards Newsletter*, *19*(1), 1–23.

Withjack, M. O., Schlische, R. W., & Olsen, P. E. (2002). Rift-basin structure and its influence on sedimentary systems. *Society for Sedimentary Geology Special Publications*, *73*, 57–81.

Zhao, G., Sun, M., & Wilde, S. A. (2002). Did South America and West Africa marry and divorce or was it a long-lasting relationship? *Gondwana Research*, *5*(3), 591–596.

SUPPORTING INFORMATION

Additional supporting information can be found online in the Supporting Information section at the end of this article.

How to cite this article: Girault, I., Basile, C., Bernet, M., Paquette, J.-L., Heuret, A., Loncke, L., Poetisi, E., & Balvay, M. (2023). Thermochronology and U–Pb dating of detrital zircons from the Demerara Plateau (French Guiana-Suriname): Implications for the provenance of the Early Cretaceous syn-rift sedimentation. *Basin Research*, *00*, 1–21. https://doi.org/10.1111/bre.12758